The Egyptian Int. J. of Eng. Sci. and Technology
Vol.14, No. 2 (May 2011)

EIJEST

AERODYNAMIC PERFORMANCE OF A HIGH-TURNING TURBINE CASCADE WITH VARYING TIP CLEARANCE*

Mohamed R. Shaalan+, Ahmed F. Abdul-gawad+, and Mahmoud A. Elewa++

+Mech. Power Engineering Department, Zagazig University, Egypt
++Sherweeda Transformer Station,Zagazig,Egypt

ABSTRACT

Modern trends in gas turbine design have been geared to produce a compact high-work-output engine as a power unit. To achieve this goal, preferring the turbine of high-turning-angle blades, the experiments focused on the effects such as lift and pressure coefficients, that to be considered when the tip clearance and incidence angle are discussed for a linear cascade. The present study aims to investigate the effect of the tip clearance on loss mechanism in turbine blades using both experimental measurements as well as CFD numerical calculations. The flow measurements are obtained using a set of calibrated five-hole probe and multi-tube manometer to measure static pressure distribution on blade surfaces, total pressure loss coefficient, velocity distribution, etc. Important points are discussed and fruitful conclusions are drawn.

KEY WORDS: cascade, turbine, tip clearance, incidence, turning angle.

PERFORMANCES AERODYNAMIQUES D'UNE CASCADE DE TURBINE HAUTE-TOURNANT AVEC UN ESPACE PERIPHERIQUE VARIABLE

RÉSUMÉ

Tendances modernes dans la conception de turbines à gaz ont été orientés à produire un compact haut de travail de sortie du moteur comme une unité de puissance. Pour atteindre cet objectif, préférant la turbine de haute tourner à angle lames, les expériences axées sur les effets tels que le transport et les coefficients de pression, que pour être considéré lorsque le jeu pointe et l'angle d'incidence sont discutés pour une cascade linéaire. La présente étude vise à étudier l'effet de la clairance astuce sur le mécanisme de perte dans les aubes de turbine utilisant les mesures expérimentales ainsi que des calculs CFD numérique. Les mesures de débit sont obtenues en utilisant un ensemble de cinq trous calibrés de la sonde et multi-tube du manomètre pour mesurer la répartition de la pression statique sur les surfaces de lame, le total des coefficients de perte de pression, de la distribution de vitesse, etc Les points importants sont discutés et les conclusions fructueuses sont dessinés.

MOTS CLÉS: cascade, une turbine, un espace périphérique, l'incidence, angle de braquage.

---

*Received : 10 /8/2010, Accepted: 24/ 5/2011 (Technical Report)

++ Contact author (elewa67@yahoo*.com*).

1. I NTRODUCTION

The aerodynamic coefficients such as lift and pressure coefficients should be considered when the tip clearance and incidence angle are discussed. A CFD model and an experimental work were developed to predict the flow characteristics for a cascade of a gas turbine blades. Profile losses , secondary flow losses and tip leakage flow are the main components of turbine blade losses. Secondary flows generated by the passage- pressure-gradients vortices represent the major source of aerodynamic losses, which account for 35%-40% of all losses investigated (Dring and Heiser [1]). Yarns, and Sjolander, [2] determined the tip leakage losses, and estimated the losses for the cascade without tip clearance. and calculated these losses as the difference between the total losses for the case with tip clearance minus the losses without tip clearance. Sieverding [3] gave an overview for different types of secondary flows in turbine blades and their effect on loss mechanism. Sjolander and Amrud [4] investigated the effect of leakage flow on the blade loading of a linear cascade. They showed the existence of separation lines on the cascade end wall and of separation bubbles on the tip surface caused by the leakage flow. Yamamoto [5] provided an information for the end-wall flow of a high-deflection turbine cascade over a range of incidence angles and tip gap heights. Bindon [6] conducted experiments on a linear cascade with tip clearance to extend the understanding of the flow physics. He measured both static pressure in the flow field and the boundary layers inside the tip gap and on the end wall. The effect of the change in incidence angle on the loss mechanism is one of the important areas when the tip clearance is present. Sjolander and Amrud [7] carried out investigations to understand the mechanism of clearance flow in the tip gap by making direct flow measurements within the gap in a linear turbine cascade at design incidence and discussed the interaction of the clearance flow with the passage vortex. Yamamoto [8] varied incidence angle when tip clearance exists. He showed that separation occurred from the pressure side of the leading edge region, and the associated loss gradually dominated the whole passage as the incidence angle is increased. His work aimed partially to overcome the lack of data at off-design conditions by providing detailed information of the end-wall flow of a high deflection turbine cascade over a range of incidence angles and tip gap heights. Bindon [9] investigated detailed development of tip clearance loss within a linear turbine cascade passage and quantified the contributions made by mixing internal gap shear flow and endwall secondary flow. El-Batsh [10] investigated the effect of tip clearance gap on the flow field within turbine blade

passage and in the tip clearance region. Paron[11] investigated the effect of secondary flow through a tow-dimensional cascade of high turning angle turbine blades. Wei, Weiyang, and Dawei[12] studied the effect of tip clearance and total pressure loss on a gas turbine performance and predicted the flow characteristics around the blades the turbine.

2. EXPERMENTAL WORK

A low speed wind tunnel located in the fluid Dynamics Laboratory Faculty of Engineering, Zagazig University. exhausting to the atmosphere was used to carry out the experimental measurements at $Re = 5.6 \times 10^4$. The present blade section is NASA-TM-82894 base profile of high-turning angle of 88° and a parabolic-arc camber line . Seven non-twisted blades were used to form the linear turbine cascade. Pressure tapping were made in the middle blade at different levels along the length of blade (2%, 25%, 50%, 75%, and 98% from root). Static pressures around the surface of the blade measured by a multi-manometer with accuracy of about 2 %. Table (1) shows the geometry and basic dimensions of tested blade cascade. The shape of the blade section is shown in Table (1). Figs.(1), (2) and (3) show the turbine cascade tested in the present work and the locations of measurements.

Table (1) Geometrical data of tested blade in cascade.

Type of blade	NASA-TM-82894
Span (H)	500 *mm*
Actual chord (ℓ)	120 mm
Aspect ratio(H/ℓ)	4.16:1
Camber turning angle(θ)	88º

A Pitot-static tube was used to measure the velocity in the test section. For the measurement of both static and stagnation pressures, a five-hole probe (Cobra type) was used (Fig (4)). It has a conical shape with 2.7 *mm* base-diameter and 0.9 *mm* tip-diameter with five measuring holes located on its tip. A centrally located pressure hole measures pressure P_1, while two lateral pressure holes measure pressures P_2 and P_3. If the probe is rotated until $P_2 = P_3$ as indicated on a manometer or other sensitive pressure indicator, the yaw angle of flow is then indicated by software program. With the yaw angle determined, an additional differential pressure ($P_4 - P_5$) is measured by pressure holes located above and below the total pressure (P_1) hole. Pitch angle is determined by calculating ($P_4 - P_5$)/ ($P_1 - P_2$). At any particular pitch angle, the velocity pressure coefficient ($P_t - P_s$)/ ($P_1 - P_2$) and total pressure coefficient ($P_1 - P_t$)/ ($Pt - Ps$) can be read from software program. The calibration curve of the five

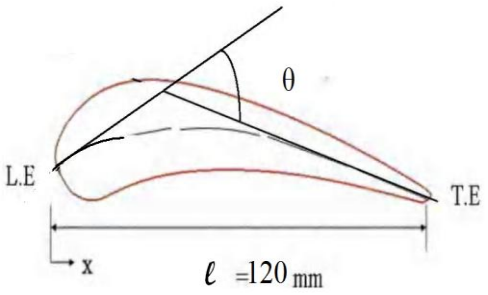

Fig (1): Geometry of Blade Section of the Present Turbine Cascade.

-hole probe is shown in Fig. (5),taken from ref [13].

It is important to be able to accurately quantify changes in the tip leakage and resulting passage vortices. Because of the small gap sizes presented here, flow measurements were restricted to the wake of the gap by a surveying probe that was located downstream of the cascade. Ensemble mean-pressure readings for the five-hole probe ports, the upstream dynamic pressure from a wall- mounted Pitot-static tube and the downstream end-wall static pressure were recorded. The probe was traversed in the span-wise and pitch-wise directions over a spatial grid of points in a two dimensional plane downstream of the cascade. Movements were oriented parallel to the blade trailing-edge plane by using a manual traverse mechanism. The linear displacement (step) in the span-wise is S/2. For the pitch-wise direction, the measurements were recorded at 2%, 25%, 50%, 75%, and 98% of the blade height (from root). The distance of the measurement- plane downstream of the test cascade was varied from x/c = 0.5, x/c = 1 to observe the spatial evolution of the tip leakage, velocity and pressure distributions. The experimental tests were planned to obtain the following data for various tip clearances:

- Profile pressure distributions
- Total pressures
- Lift and drag coefficients

Table (2): Geometrical data of tested cascade

Solidity ($\sigma = \ell / s$)	1.35
Number of blades	7
Stager angle (γ) degree	45º
Tip clearance (H%)	0%,2%,4%
Blade spacing (mm)	88.8
Axial chord (mm)	88.8
$\alpha`_1, \alpha 2$ (degree)	21º,67º

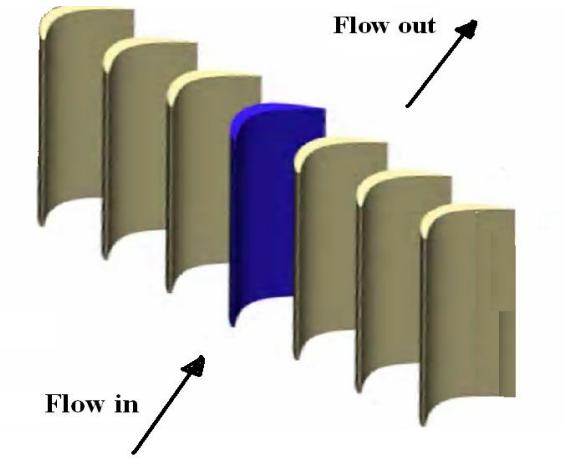

Fig(2)| Blades in cascade

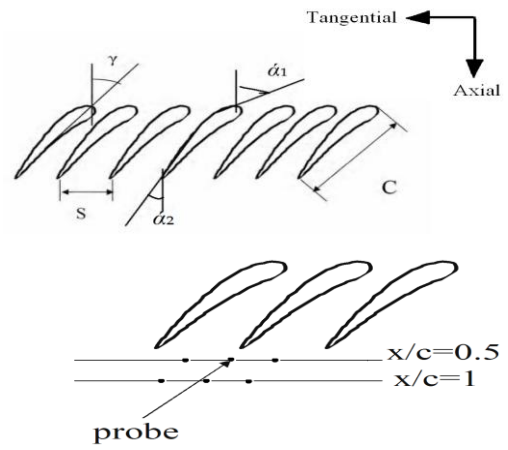

Fig. (3) Geometrical Details of Tested Cascade Showing Locations of Measurement Planes at Exit.

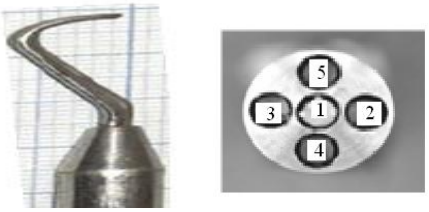

Fig(4): Photo of Measuring Head of Five Hole Probe

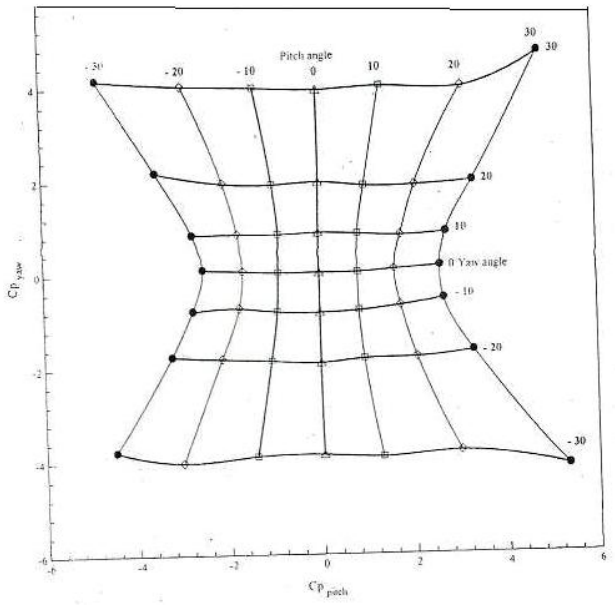

Fig.(5): Five-hole Probe Calibration Chart (from ref [13])

3. NUMERICAL TREATMENT

The flow field is obtained by solving equations for steady incompressible flow. Since the flow field is repeated, the flow is solved in one flow passage between two consecutive blades.

3.1 Governing Equations

The governing equations consist of the well-known set of partial differential equations . These equations include the so-called conservation of mass, conservation of momentum and turbulent viscosity, which have two turbulence transport equations, one for the turbulent kinetic energy and the other for the dissipation rate. The governing equations of flow field as well as standard *K-ε* model are given as follows:

-Mass conservation equation

The mass conservation equation for steady flow is given by:

$$\frac{\rho}{t} + \frac{\partial U_j}{\partial x_j} \quad 0 \qquad (1)$$

Where; *J* is a tensor indicating 1, 2, and 3, U_j is the velocity in the j^{th} direction and X_j is the coordinate in the j^{th} direction.

-Momentum conservation equation

$$\frac{\partial U}{\partial t} + \frac{\partial}{\partial x_j}(U_j U_i) = -\frac{1}{\rho}\frac{\partial P}{\partial x_i} + \frac{\partial}{\partial x_j}(\nu \frac{\partial U_i}{\partial x_j} - \overline{u_i u_j}) \qquad (2)$$

Where; *P* is the static pressure, ν is the air kinematics viscosity, $\overline{u_i u_j}$ is given by:

$$-\overline{u_i u_j} \qquad 2\nu_t D_{ij} - \frac{2}{3}K\delta_{ij} \qquad (3)$$

Where, ν_t is the turbulence kinematics viscosity that is given by:

$$\nu_t = \frac{C_\mu K^2}{\varepsilon} \quad (4)$$

and, $$D_{ij} = \frac{1}{2}\left(\frac{\partial U_i}{\partial x_j} \quad \frac{\partial U_j}{\partial x}\right) \quad (5)$$

Where; C_μ is a constant that equals 0.07, K is the turbulence kinetic energy, ε is the dissipation rate of turbulence kinetic energy, δ_{ij} is the Kronecker delta.

-Turbulence kinetic energy equation

$$-\frac{\partial}{\partial x_j}\left(U_j K\right) = \frac{\partial}{\partial x_j}[(\frac{\upsilon_t}{\mathrm{Pr}_k} + \upsilon)\frac{\partial K}{\partial x_j}] - \overline{u_i u_j} D_{ij} - \varepsilon \quad (6)$$

Where; Pr_k is the Prandtl number for turbulence kinetic energy.

-Dissipation rate of turbulence kinetic energy

$$\frac{\partial}{\partial x_j}(U_j \varepsilon) = \frac{\partial}{\partial x_j}[(\frac{\upsilon_t}{\mathrm{Pr}_\varepsilon} + \upsilon)\frac{\partial \varepsilon}{\partial x_j}] + C_1 \frac{\varepsilon}{K}(-\overline{u_i u_j} D_{ij}) - C_2 \frac{\varepsilon^2}{K} \quad (7)$$

Where; Pr_ε is Prandtl number for dissipation rate of turbulence kinetic energy, C_1 is a model constant that equals 1.44; C_2 is a model constant that equals 1.92. This study using the commercial code Fluent 6.3.

3.2 Computational Grid

Gambit is the software, which combines the features of both modeling and meshing. The computational domain is shown in Fig. (6). The tetrahedral mesh type was used in the present work. The mesh is very fine next to the solid boundary of the blade. The size of the element increases away from the solid boundaries. Careful consideration was paid to minimize the dependence of the solution on the mesh by improving the clustering of cells near solid walls until results are almost constant. The investigation was preliminary carried out using different numbers of cells, namely: 80,000, 100,000, and 120,000. It was found that a number of cells in the range of 100,000 gives the best results in comparison to with experimental findings. So, there was no need to increase the number of cells above 100,000. The least y^+ from the wall for the first node was about 4. The mesh for the cross section of the blade is shown in Fig. (7).

3.3 Boundary Conditions

The boundary conditions are expressed as the values of the velocities, pressures, turbulence kinetic energy, and turbulence kinetic energy dissipation at the boundaries of the computational domain.

Boundary conditions can be listed as:

(1) The velocity at upstream boundary is uniform, so $u=U_\infty$.

(2) The boundary at the sides is symmetric.

(3) The no-slip and no-penetration conditions are used on the surfaces of the blade, so $U_i=0$.

(4) The zero gradient condition is assumed for all variables at downstream boundary, so $\partial U_i/\partial x=0$

(5) The value of K and ε at inlet to domain are 0.4704 m^2/s^2 and 0.4912 m^2/s^3, respectively.

The law of the wall was used as a standard wall function.

4. RESULTS

4.1 Pressure Distributions

In Figs. (8-a) and (8-b) at zero incidence angle for the suction side, it is seen that there is no large effect at different tip clearances on distribution of C_P at 50 % and 75 % span. But C_P decreases with the tip clearance at heights of 75% and 98 %. For

the pressure side, the minimum value of C_P is found at x/c = 0.3, 0.35 and 0.75 at heights of 50 %, 75 % and 98%, respectively. The separation occurs at x/c = 0.3 for 50 % and 75 % span, and 0.7 for 98% span. For the positive incidence angle, Figs. (8-c)-(8-f), there is no effect on C_P on the suction and pressure sides at 50 % span. The separation occurs at x/c = 0.4 on the suction side. The values of C_P decrease slightly with tip clearance from the leading edge to the trailing edge on the pressure side for positive angles. Also, C_P decreases with tip clearance till x/c =0.73 for $\alpha = 15^o$, on the suction

side then increases gradually till the trailing edge. For the negative incidence angle, Figs. (8-g)-(8-j), there is no effect of C_P on the suction and pressure sides at 50 % span. The separation occurs at x/c = 0.44 on the suction side. The values of C_P decrease with tip clearance from the leading edge to trailing edge on the pressure side for negative angles. The separation occurs at x/c = 0.3 for all incidence angle. Also, C_P decreases with tip clearance till x/c = 0.65 for $\alpha = -15^o$ on the suction side then increases gradually till the trailing edge. Concerning the experimental results, we find a good agreement with the computational predictions. The agreement is demonstrated in decreasing *Cp* with the tip clearance and that no effect on C_P on the suction and pressure sides at 50 % span for all incidence angle and also in locating the separation point.

4.2 Lift Coefficient

The lift coefficient can be calculated from the pressure distribution by numerical integration as:

$$C_l = \int_{LE}^{TE} (C_{pl}(x) - C_{pu}(x))\, d\frac{x}{c} \qquad 8$$

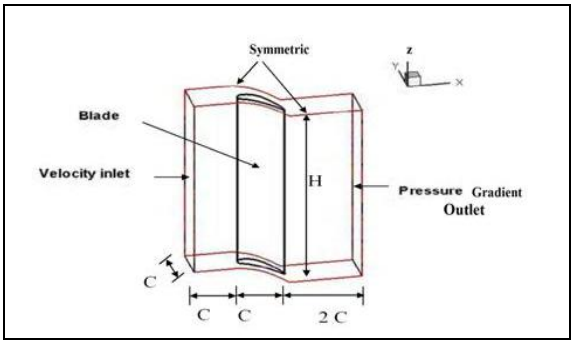

Fig. (6): Computational Domain and Boundary Conditions.

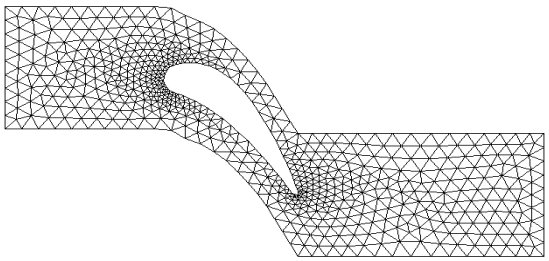

Fig. (7): Mesh in the Computational Domain

lower surface, C_{pu} is the pressure coefficient on the upper surface, *LE* is the leading edge, *TE* is the trailing edge. The maximum value of the lift coefficient is attainable with high turning blade angle in high lift region. Different types of flow separation occur depending on blade shape. Trailing edge flow separation represents the dominating effect. Generally, flow separation results in a reduction of the lift curve slope before maximum lift, whereas, in the post-stall region a considerable loss of blade lift occurs. where; C_{pl} is the pressure coefficient on the As shown in Fig. (9),The lift coefficient decreases with tip clearance. increases beyond 10°.Where the lift begins to halt or decrease. As tip clearance is increased C_L too is reduced. However, at the negative angle α = -15°, Maximum lift occurs at $\alpha \approx 10^o$. The stall appears to occur the incidence angle

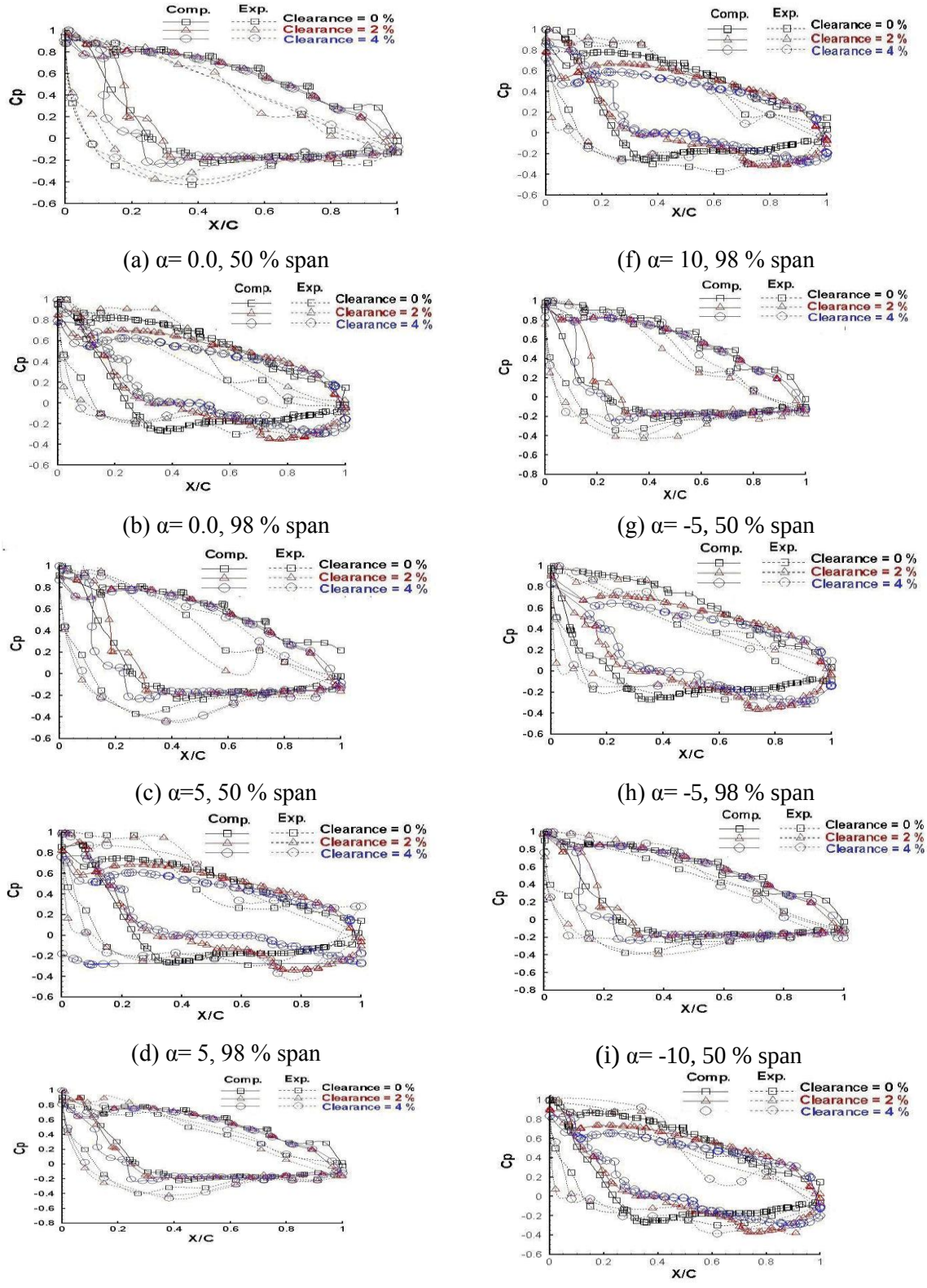

(a) α= 0.0, 50 % span

(b) α= 0.0, 98 % span

(c) α=5, 50 % span

(d) α= 5, 98 % span

(e) α= 10, 50 % span

(f) α= 10, 98 % span

(g) α= -5, 50 % span

(h) α= -5, 98 % span

(i) α= -10, 50 % span

(j) α= -10, 98 % span

Fig.(8): Experimental versus Computational Pressure Distributions (C_p) for Different Tip Clearances

a small effect of tip clearance on C_L is noticed. At the positive angle α = +15°, the change of C_L with tip clearance is noticeable, values of C_L decreasing with the tip clearance. However, at α = - 15 there is a noticeable effect on C_L at 4% tip clearance, C_L decreasing to 0.3. With the decrease of incidence angle to -10°, C_L increases to 0.4 for 0 % and 2% tip clearances and to 0.5 for 4% tip clearance. At 0.0% tip clearance, C_L steadily increases starting from α = -10° and reaches a maximum value of 0.78 at α = + 5°. Then, it decreases at α = +10° to 0.62. The maximum value of C_L for all clearances can be found somewhere between the positive angles 5° and 10°. A zero lift appears to occur in computationally at α = -18° and appears in experimental results at α = -19° (see Fig(9)).

4.3 Critical Incidence Angle

Increasing the incidence angle is associated with increasing of lift coefficient up to a maximum value (critical incidence). At the critical incidence, the air begins to flow less smoothly over the blade suction side and begins to separate. As the incidence angle increases, the separation point of the air moves from the trailing edge towards the leading edge. Above the critical incidence angle, nearly the whole of the suction side flow is separated and blade then fails to produce more lift. As incidence angle is further increased.Therefore,the critical incidence angle is the incidence angle where maximum lift occurs. This may also be called the "stall angle". In the present work, the critical angle is approximately at α = + 10 degrees (seen Fig. (9)).

4.4 Drag Coefficient

The drag coefficient C_d is defined as:

$$C_d = D / (A \times .5 \times \rho \times U^2) \qquad (9)$$

Concerning experimental results, C_d is calculated by integrating forces caused by the pressure variations along blades. For small incidence angle -5 and +5, drag is nearly constant as shown in Fig. (10) for all tip clearances. As the angle increases from +5 to +10, the drag coefficient increases. This is due to the increased frontal area and increased boundary layer thickness. At zero incidence angle, a small amount of drag is generated by skin friction and blade form..

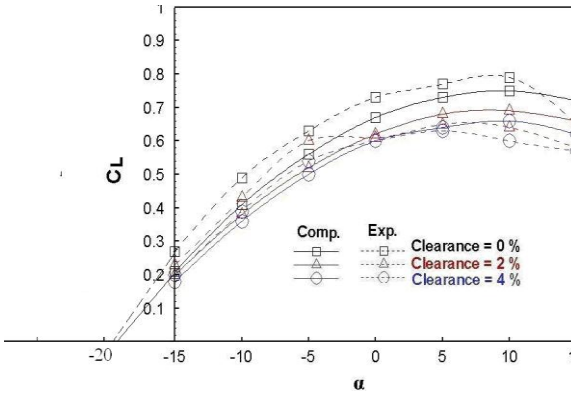

Fig (9): Experimental versus Computational Variation of Lift Coefficient with α for Different Tip Clearances

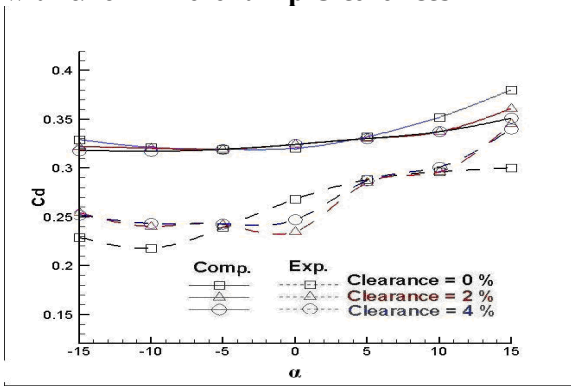

Fig. (10) Drag Coefficient at Different Incidence Angles and Different Clearance

4.5 Total Pressure Contours and Loss Coefficient

The values of total pressure decrease with incidence angle for the pressure side and decrease on the suction side at all levels of span except at 98% where the total pressure is constant for tip clearance 0.0% as shown in Fig. (13). For tip 4%, it is found as shown in Fig. (14) that the total pressure increases on the suction side at all levels of span except at 98 % where it decreases. For 0.0% tip clearance, the total pressure appears to be constant for negative incidence angle and decreases with positive angles. However, at α = 15°, it decreases to the lowest value, and with increasing the tip clearance the total pressure decreases.

Fig (11) shows the total-pressure loss coefficient caused by the tip clearance flow.

$$\xi = \frac{P_{inlet} - P_{outlet}}{\frac{1}{2}\rho U^2}$$

. It could be found that the mass-averaged total-pressure-loss coefficients vary in approximately linearly with in the tip clearance. The increase of tip clearance causes the total-pressure loss to increase. Good agreement is noticed with the corresponding case of ref [12].

5. EXPERIMENTAL VERSUS COMPUTATIONAL RESULTS AND COMPARISON WITH PREVIOUS INVESTIGATION

Fig. (12) shows comparisons between the values of CP that obtained from computational predictions and that found from the experimental investigations in the case of zero incidence and no clearance. It is obvious that the computed distributions of CP on the pressure and suction side compare well with experimental data and with ref [11].

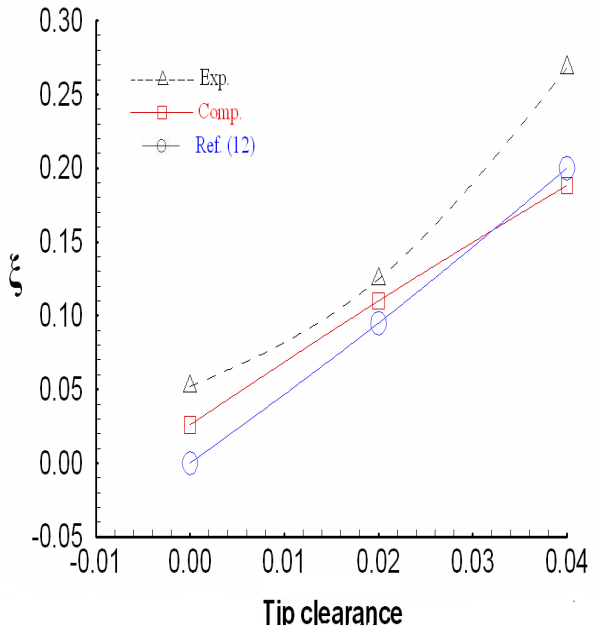

Fig(11) Total Pressure Loss vs. Tip Clearance Height

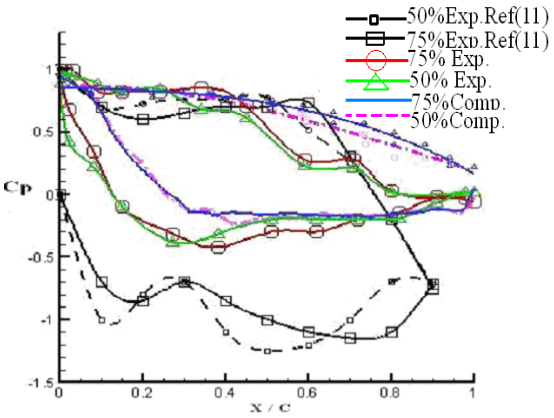

Fig(12): Comparisons between Experimental Results and Computational Predictions for the Values of C_P (α = 0°) .

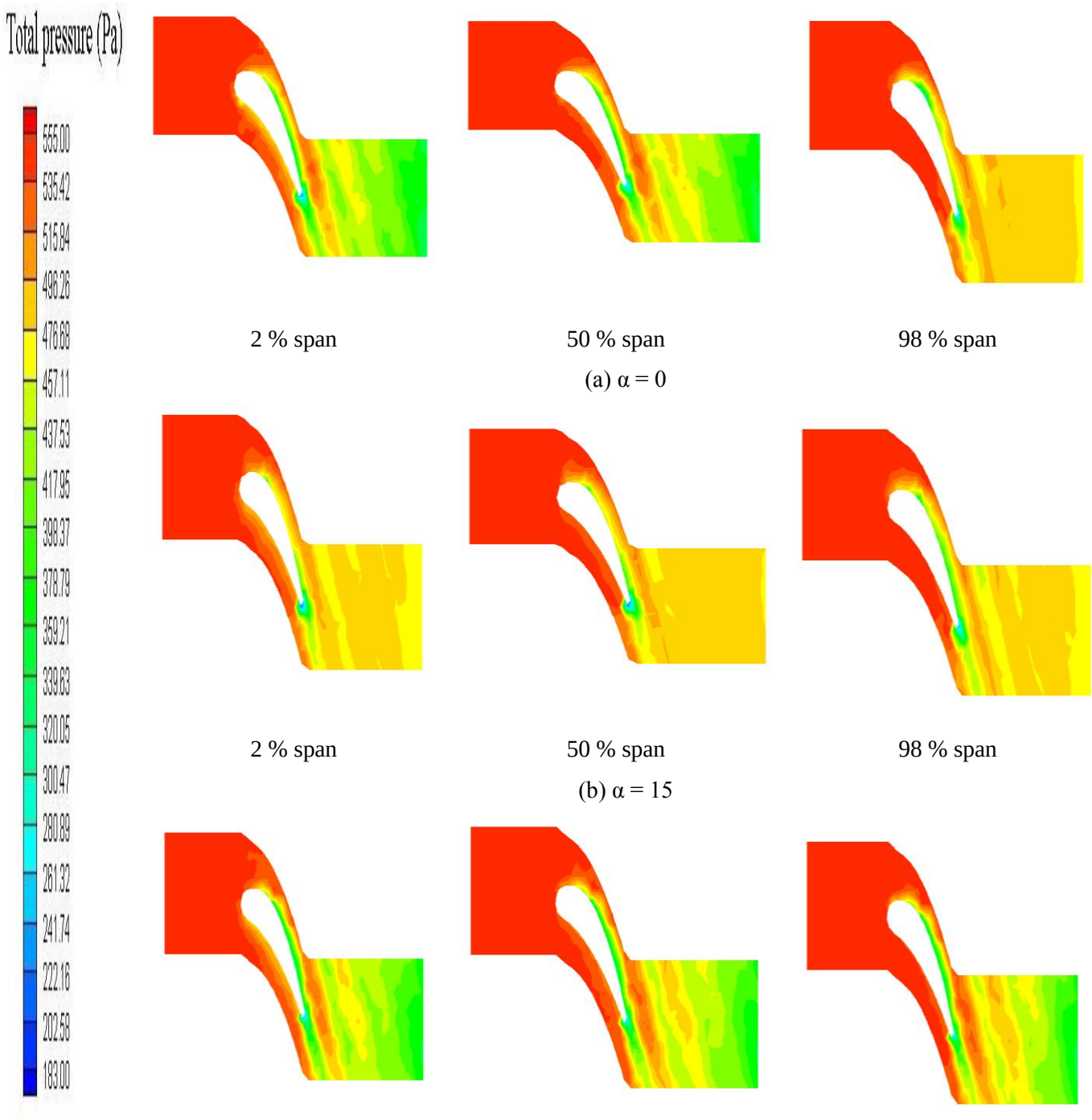

Fig. (13) Variation of Total Pressure Contours with Incidence Angle at Zero Tip Clearance for Various Blade Sections along Span.

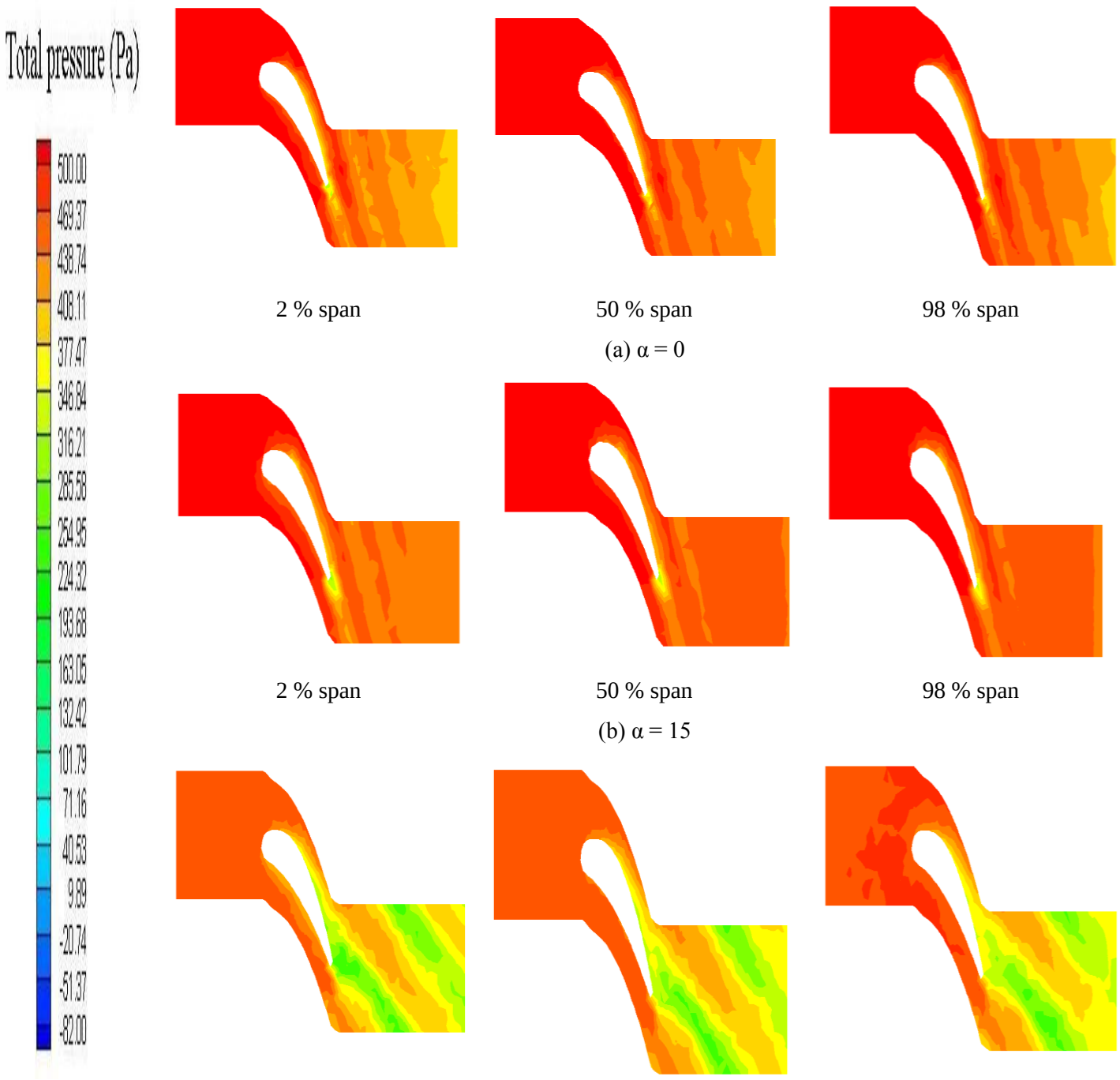

2 % span 50 % span 98 % span

(a) α = 0

2 % span 50 % span 98 % span

(b) α = 15

2 % span 50 % span 98 % span

(c) α = -15

Fig. (14) Variation of Total Pressure Contours with Incidence Angle at 4 % Tip Clearance for Various Blade Sections along Span.

6. CONCLUSIONS

Three-dimensional flow through a high turning turbine-blade-cascade of a gas turbine was investigated taking the effect of tip clearance into consideration. Different values of tip clearances were considered for effect on losses and lift coefficient. Based on the above results discussion, the following points can be concluded:

1-The lift coefficient decreases with tip clearance and maximum critical lift occurs at α = 10^o (stall occurs when α goes beyond +10^o).

2- For zero incidence angle, for suction side, C_P decreases with the tip clearance at 75% and 98% span. For the pressure side, the separation occurs at x/c = 0.3 at 50% and 75% span, whereas, it occurs at x/c = 0.7 at 98% span.

3- For negative incidence angle, separation occurs at x/c = 0.44 on the suction side. C_P decreases with tip clearance to reach a minimum at x/c = 0.65 for α = -15^o on the suction side then increases gradually till the trailing edge.

4- For positive incidence angle, separation occurs at x/c = 0.4 on the suction side. On the suction side, C_P decreases with tip clearance to reach a minimum at x/c =0.73 for α=15^o then increases gradually till the trailing edge.

5- Total pressure decreases with incidence angle from -15^o to 15^o for the pressure side and decreases on the suction side at all levels of span except at 98% span.

6- A zero lift appears to occur computationally predictions at -18^o, whereas, it appears to occur experimentally at -19^o.

7- For small incidence angles (-5 and +5), drag is nearly constant at all tip clearances.

8- The deflection decreases with tip clearance. At α=-15^o, the deflection is highly affected. For small incidence angle at no clearance, the deflection is nearly constant

Nomenclature

A	Frontal area
C_L	Lift coefficient
C_d	Drag coefficient
C_μ	Constant equals 0.07
Cp	Pressure coefficient

$$C_p = \left(\frac{P - P_\infty}{0.5\rho U^2}\right)$$

C up, CpL	Pressure coefficients on the upper and lower surface, respectively
C_1, C_2	model constant
D	drag force (N)
H	Span length (mm)
J	Tensor indicator
K	Turbulence kinetic energy
ℓ	Chord length (mm)
L	Lift force (N)
P_1, P_2, P_3, P_4, P_5	Pressures measured by five-hole probe
P_s	Static pressure
P_∞	Free-stream static pressure
Pr	Prandtl number
Pt	Total pressure
S	Blade or pitch spacing (mm)

U_j Velocity in the j^{th} direction

U_∞ Up-stream velocity(m\s)

X_j Coordinate in the j^{th} direction (mm)

x Axial coordinate (mm)

y Tangential (pitchwise) coordinate(mm)

Greek symbols:

α Incidence angle (degree)

α_1, α_2 Flow inlet and exit angles, respectively (degree)

$\alpha`_1, \alpha`_2$ Blade inlet and exit angle, respectively (degree)

γ Stagger angle (degree)

δ Deviation (degree)

ε Dissipation rate (m^2/s^{3})

ξ Total pressure loss coefficient

θ Camber angle (degree) (turning angle)

ν Kinematic viscosity (m²/s)

ν_t Turbulence kinematic viscosity

σ Solidity (= l /S)

3 Deflection (degree)

ρ Air density (1.225 kg / m^3 at sea level and 15 C°)

Subscripts:

Max. Maximum

Def. Deflection

TM Technical Memo

REFERENCES

1. Dring, R. P., and Heiser, W. H., "Aerothermodynamics of Aircraft Engines Components", (Chap.4 "Turbine Aerodynamics", AIAA Education Series, New York: AIAA Inc., 1985.

2. Yarns, M.I., and Sjolander, S.A., "Development of the Tip Leakage Flow Downstream of a Plane Cascade of Turbine Blades: Vorticity Field," ASME, Journal of Turbomachinery, Vol. 113, p. 609, 1990.

3. Sieverding, C. H. "Recent Progress in the Understanding of Basic Aspects of Secondary Flows in Turbine Blade Passages," ASME Journal of Engineering for Gas Turbines and Power, Vol.107, pp. 248-257, 1985.

4. Sjolander, S. A., and Amrud, K. K., "Effects of Tip Clearance on Blade Loading in a Plane Cascade of Turbine Blades," ASME Journal of Turbo machinery, Vol. 109, pp. 237–245, 1987.

5. Yamamoto, A., "Production and Development of Secondary Flows and Losses within Two Types of Straight Turbine Cascades: Part 1–A Stator Case," ASME Journal of Turbomachinery, Vol. 109, 1987, pp. 186–193.

6. Bindon, J. P., "The Measurement and Formation of Tip Clearance Loss," ASME Journal of Turbomachinery, Vol. 111, pp. 257–263, 1989.

7. Sjolander, S.A., and Amrud, K.K., "Effects of Tip Clearance on Blade Loading in a Plane Cascade of Turbine Blades," ASME, Journal of Turbomachinery, 109, p. 237, 1987.

8. Yamamoto, A. "End Wall Flow/Loss Mechanisms in a Linear Turbine Cascade with Blade Tip Clearance," ASME Journal of Turbo machinery, Vol. 111, pp. 264–275, 1989.

9. Bindon, J. P., and Morphis, G., "The Development of Axial Turbine Leakage Loss for Two Profiled Tip Geometries Using Linear Cascade Data", ASME Journal of Turbo machinery, Vol. 114, pp. 198-203, 1992.

10. El-Batsh, H., Bassily, M., and Sherif, M. F., " Experimental And Numerical Study of The Effect of Tip Clearance on Three-dimensional Flow Field Through Linear Turbine Cascade", Eigth International Congress of Fluid Dynamics &Propulsion, Sharm-Elshiekh, Egypt, December, 2006.

11. Paron, G. J. and Eng, B.,"Secondary Flow in a Two-Dimensional cascade of High Turning Turbine Blades, "M.S. Thesis, Hamilton University, Ontario, Canada, April, 1981.

12. Wei, L., Weiyang, Q., and Dawei, S., “Tip Clearance Flow in Turbine Cascades", Chinese Journal of Aeronautics, Vol. 22, PP 193-199, 2008.

13. Hasanean M. E-s. M. "Experimental Investigation of Fluid and Heat Transfer Around Circular Cylinder-Flat and Curved Plates Combinations" Ph, D, Thesis, Cairo University, 1988.